HHS Public Access

Author manuscript

J Control Release. Author manuscript; available in PMC 2015 August 10.

Published in final edited form as:

J Control Release. 2015 May 10; 205: 134–143. doi:10.1016/j.jconrel.2015.01.005.

pH-sensitive oncolytic adenovirus hybrid targeting acidic tumor microenvironment and angiogenesis

Joung-Woo Choi[a], **Soo-Jung Jung**[a], **Dayananda Kasala**[a], **June Kyu Hwang**[a], **Jun Hu**[b], **You Han Bae**[b,c,*], and **Chae-Ok Yun**[a,**]

You Han Bae: you.bae@utah.edu; Chae-Ok Yun: chaeok@hanyang.ac.kr

[a]Department of Bioengineering, College of Engineering, Hanyang University, 222 Wangsinmi-ro, Seongdong-gu, Seoul, Republic of Korea

[b]Department of Pharmaceutics and Pharmaceutical Chemistry, The University of Utah, 30S 2000 E, Room 2972, Salt Lake City, UT 84112, USA

[c]Utah-Inha Drug Delivery Systems (DDS) and Advanced Therapeutics Research Center, 7-50 Songdo-dong, Yeonsu-gu, Incheon 406-840, Republic of Korea

Abstract

Although oncolytic adenoviruses (Ads) are an attractive option for cancer gene therapy, the intravenous administration of naked Ad still encounters unfavorable host responses, non-specific interactions, and heterogeneity in targeted cancer cells. To overcome these obstacles and achieve specific targeting of the tumor microenvironment, Ad was coated with the pH-sensitive block copolymer, methoxy poly(ethylene glycol)-*b*-poly(L-histidine-co-L-phenylalanine) (PEG*b*PHF). The physicochemical properties of the generated nanocomplex, Ad/PEG*b*PHF, were assessed. At pH 6.4, GFP-expressing Ad/PEG*b*PHF induced significantly higher GFP expression than naked Ad in both coxsackie and adenovirus receptor (CAR)-positive and -negative cells. To assess the therapeutic efficacy of the Ad/PEG*b*PHF complex platform, an oncolytic Ad expressing VEGF promoter-targeting transcriptional repressor (KOX) was used to form complexes. At pH 6.4, KOX/PEG*b*PHF significantly suppressed VEGF gene expression, cancer cell migration, vessel sprouting, and cancer cell killing effect compared to naked KOX or KOX/PEG*b*PHF at pH 7.4, demonstrating that KOX/PEG*b*PHF can overcome the lack of CAR that is frequently observed in tumor tissues. The antitumor activity of KOX/PEG*b*PHF systemically administered to a tumor xenograft model was significantly higher than that of naked KOX. Furthermore, KOX/PEG*b*PHF showed lower hepatic toxicity and did not induce an innate immune response against Ad. Altogether, these results demonstrate that pH-sensitive polymer-coated Ad complex significantly increases net positive charge upon exposure to hypoxic tumor microenvironment, allowing passive targeting to the tumor tissue. It may offer superior potential for systemic therapy, due to its

*Correspondence to: Y.H. Bae, Department of Pharmaceutics and Pharmaceutical Chemistry, University of Utah, Skaggs Research Building, Rm 2972, 30S, 2000E, Salt Lake City 84112, USA. Tel.: +1 801 585 1518; fax: +1 801 585 3614. **Correspondence and Reprint request to: Dr. Chae-Ok Yun, Department of Bioengineering, College of Engineering, Hanyang University, 222 Wangsinmi-ro, Seongdong-gu, Seoul, Republic of Korea. Tel: +82 2 2220 0491; fax: +82 2 2220 4850.

Appendix A. Supplementary data: Supplementary data to this article can be found online at http://dx.doi.org/10.1016/j.jconrel.2015.01.005.

improved tumor selectivity, increased therapeutic efficacy, and lower toxicity compared to naked KOX.

Keywords

Cancer gene therapy; Oncolytic adenovirus; pH-sensitive polymers; Tumor microenvironment; Systemic administration; Hypoxia

1. Introduction

Among the various cancer treatment strategies, oncolytic adenoviruses (Ads) are a promising therapeutic strategy with numerous biochemical advantages. First, oncolytic Ads specifically infect cancer cells, which often have defects in the factors that guard against viral replication, such as endogenous tumor suppression proteins (p53, pRb, p14ARF, etc.) [1–6]. Second, oncolytic Ads destroy host cells at the end of their lytic cycles and spread 1000–10,000 viral progeny copies per cell, leading to further infection and subsequent eradication of neighboring cancer cells [7]. Third, oncolytic Ads are potent and efficient viral vectors in both dividing and non-dividing cells, and can be concentrated at high titers [8]. All Ad serotypes except group B, use coxsackie and adenovirus receptor (CAR) to initiate cell binding. Subsequent interaction between an RGD motif at the penton base protein of Ad with cell integrins ($\alpha_v \beta_1$, $\alpha_v \beta_3$, or $\alpha_v \beta_5$) allows for virus entry through clathrin-mediated endocytosis. Despite these advantages, however, issues with immunogenicity and CAR dependency to infect cells must be overcome before Ads can be developed as therapeutic agents against metastatic cancers.

These issues are magnified when Ads are delivered systemically. Intravenously delivered Ads are inactivated and cleared by both innate and adaptive immune responses, limiting the benefit of repeated or high-titer administrations of Ad [9]. Moreover, the non-specific liver accumulation of Ads by Kupffer cells and the interactions of Ads with platelets and erythrocytes [10–12] lead to toxic interactions, the quick elimination of Ads, and generally low antitumor effects [13]. In order to be successful, however, an Ad-based therapy against both primary and metastatic cancers must be able to be administered systemically. Thus, alternative strategies that utilize hybrid systems (i.e., combinations of viral and non-viral systems) have been proposed [14].

Hybrid systems utilizing viral surface modifications have been explored for their potential to overcome biochemical and immunological barriers. There are two main strategies for surface modification of Ads. In the first, free amines are conjugated onto the surface of Ads using functional polymers such as polyethylene glycol (PEG) [15,16], arginine-grafted bioreducible polymer (ABP) [17,18], or N-(2-hydroxy-propyl) methacrylamide [19,20]. This strategy allows the complex to evade capture by immune cells and neutralization antibodies, increasing its plasma circulation while decreasing liver toxicity and the immune response. However, this covalent conjugation abrogates CAR-mediated endocytosis because the Ad fibers (which are crucial to cell entry) are obstructed by steric hindrance from the polymeric chains. To improve upon these issues, PEGylated Ad surface complexes have been further conjugated with active targeting moieties, such as antibodies, growth factors, and small

peptides [9,21–25]. However, such active targeting strategies have yielded only modest antitumor efficacy, largely because the targeting reactions do not cover all the heterogeneous cell morphologies, phenotypes, properties, antigen expression patterns, and inherent/acquired drug resistances of tumor tissues [26]. For example the monoclonal antibody, Herceptin, specifically binds to the HER2/neu receptor and is widely used to treat both metastatic and early breast cancer. However, HER2/neu is only overexpressed in 20–30% of breast cancer patients [9], making Herceptin-based strategies ineffective in many cases.

The second strategy for surface modification is to use electrostatic interactions to join positively charged polymers, such as polyethylenimine [27], ABP [18], poly(amido amine) [28], chitosan [29] or methoxy poly(ethylene glycol)-b-poly{N-[N-(2-aminoethyl)-2-aminoethyl]-L-glutamate} [30], with the negatively charged Ad surface. Ad–cationic-polymer complexes have net positive zeta potentials, and thus can interact with negatively charged cell membranes for enhanced internalization. Moreover, the cationic polymer coating can easily dissociate in endosomes, effectively releasing the Ads through the proton-sponge effect [31]. For example, ABP, which has reducible disulfide bonds in the backbone, has been shown to greatly improve the transduction efficiency of Ads while lowering their therapeutic cytotoxicity [18]. However, positively charged Ad/polymer complexes possess poor tumor selectivity due to their nonspecific uptake and interactions with negatively charged cell membranes [32], limiting the overall effectiveness of such therapies. Thus, despite the advantages of these Ad-surface modification strategies, we need new targeting methods that can exploit a consistent characteristic of tumor tissues.

Tumors exhibit increased proliferation and angiogenesis, and thus their microenvironments differ from those of normal tissues. Tumor tissues are often hypoxic (lacking adequate oxygen) and characterized by a lower pH relative to non-tumor tissues [33]. Hypoxia is generally considered to be a negative factor in cancer, as it contributes to chemoresistance and metastasis. It is rare in normal tissues, however, meaning that hypoxia and low pH could potentially be targeted by anti-cancer drugs. To our knowledge, however,no previous study has reported a detailed investigation of a hypoxia-responsive oncolytic Ad-nanoparticle-hybrid delivery system for cancer therapeutics.

In this study, Ads coated with a pH-responsive histidine moiety-containing polymer, methoxy poly(ethylene glycol)-*b*-poly(L-histidine)-poly(L-phenylalanine) (3.3 K, PHF; H:F = 23:1) (abbreviated as PEG*b*PHF) [34], were generated using electrostatic interactions between the positively charged cationic polymer and the negatively charged surface of the Ad. Designated Ad/PEG*b*PHF, these complexes were investigated for their ability to target and exhibit therapeutic efficacy to hypoxic tumor microenvironments. We hypothesized that: 1) Ad/PEG*b*PHF would show long-term circulation in the blood (neutral pH; 7.4) due to the immune-masking effect of PEG; and 2) Ad/PEG*b*PHF, which has a pK_a value of around 6.5, would undergo protonation of the imidazole ring in its histidine portion upon exposure to the hypoxic tumor microenvironment, facilitating the cellular uptake due to strong bind affinity with negatively charged cell membrane, triggering the endosomal escape of complex, and releasing the Ads into cytosol. Collectively, our results show for the first time that oncolytic Ad/PEG*b*PHF can target the hypoxic tumor microenvironment and improve the therapeutic efficacy of hybrid oncolytic Ad nanocomplexes in vitro and in vivo.

2. Materials and methods

2.1. Cell culture and preparation of Ad

All cell lines were cultured in Dulbecco's modified Eagle's medium (DMEM; GIBCO-BRL, Grand Island, NY) supplemented with 10% fetal bovine serum (FBS; GIBCO-BRL) at 37 °C in a humidified atmosphere containing 5% CO_2. A human embryonic kidney cell line expressing the Ad E1 region (HEK 293), two human brain cancer cell lines (U343 and U87), a lung cancer cell line (A549), and a human breast cancer cell line (MCF7) were purchased from the American Type Culture Collection (ATCC, Manassas, VA). The in vitro adenoviral gene delivery efficiency was examined with a green fluorescence protein (GFP)-expressing Ad E1A gene-deleted replication-incompetent Ad (dE1/GFP) [18,25]. KOX, which is a VEGF promoter-targeting transcriptional repressor zinc-finger protein-expressing oncolytic Ad with a mutated E1A region and a deletion of the E1B region, was generated and characterized as previously described [35,36]. KOX and dE1/GFP were propagated in HEK293 cells and purified by the CsCl gradient method. TheAd viral particle (VP) number was estimated by measuring the optical density at 260 nm (OD_{260}), for which an absorbance value of 1 was equivalent to $1 \times 1.1 \times 10^{12}$ viral particles/mL (VP/mL) [37]. Purified viruses were stored at −80 °C until use.

2.2. Physicochemical characterization of naked Ad and Ad/PEG*b*PHF complexes

The average size and zeta potential of the Ad/PEG*b*PHF complexes were measured with a Zetasizer 3000HS (Malvern Instruments, Inc., Worcestershire, UK) with a He–Ne laser beam (633 nm, fixed scattering angle of 90°) at 25 °C. Electrostatic complexation of dE1/GFP with PEG*b*PHF was performed at molar ratios ranging from 5×10^4 to 1×10^6 polymer molecules/Ad particle at pH 7.4. Briefly, various molar ratios of PEG*b*PHF were mixed with Ad (1×10^{10} VP), gently aspirated with a pipet tip, and incubated at room temperature for 30 min. HEPES (H0887; Sigma, St. Louis, MO) was added to a final volume of 1.0 mL prior to analysis. The sizes and zeta potential values are presented as means and standard deviations from three measurements.

2.3. Gel-retardation assay

To assess the Ad-encapsulating ability of PEG*b*PHF, various molar ratios (5×10^4 to 1×10^6) of PEG*b*PHF-coated Ad at pH7.4 were prepared and resolved by 0.8% (w/v) agarose gel electrophoresis at 80 V for 30 min in 1 × TAE buffer pH 8.0 [10.0 mM Tris/HCl (pH 7.6), 1% (v/v) acetic acid, and 1.0 mM EDTA (pH 8.0)] containing ethidium bromide (E1510, Sigma). The resolved viral DNA was visualized using a ChemiDoc gel documentation system (Syngene, Cambridge, UK).

2.4. Transmission electron microscopy (TEM) imaging

The naked dE1/GFP and dE1/GFP/PEG*b*PHF complexes (molar ratio, 1×10^6) were incubated for 30 min, and morphologies were characterized by TEM (JEM-2000EXll, JEPL; Nikon, Tokyo, Japan) at 200 kV.

2.5. Assaying the transduction efficiency of dE1/GFP/PEG*b*PHF

The transduction efficiencies of dE1/GFP or dE1/GFP/PEG*b*PHF complexes of different molar ratios were measured by fluorescent microscopic quantification of GFP expression and fluorescence-activated cell sorting (FACS) analysis in CAR-positive U343 and A549, and CAR-negative MCF7 cells. Each cell line was seeded at a density of 1×10^5 cells/well in a 12-well plate. After 24 h, the cells were transduced with naked dE1/GFP or dE1/GFP/PEGbPHF, using 10 (U343, A549) or 100 (MCF7) MOI at pH 7.4 or pH 6.4 for 45 min, then changed with 5% FBS containing media. Similarly, the transduction efficiency of dE1/GFP/PEGbPHF complexes at different pHs (6.4, 6.6, 6.8, 7.0, 7.4), were also measured in CAR-positive (U343 and A549) and CAR-negative (MCF7) cells. After 48 h of transduction at 37 °C, the cells were observed with a fluorescence microscope (Olympus IX81; Olympus Optical, Tokyo, Japan). Cells were also viewed with a BD FACScan analyzer (Becton-Dickinson, San Jose, CA) and assessed with the CellQuest software (Becton-Dickinson). The data are presented as the means and standard deviations of three measurements.

2.6. VEGF quantification

KOX is an oncolytic Ad expressing VEGF promoter-targeting transcriptional repressor zinc-finger protein which can suppress VEGF expression. Thus, we evaluated the VEGF level upon infection with either KOX or KOX/PEG*b*PHF. The expression levels of VEGF were quantified using a human VEGF Quantikine Immunoassay kit (R&D Systems, Minneapolis, MN), according to the manufacturer's recommendations. Serial dilutions of a known purified recombinant human VEGF were used to establish a standard curve. Briefly, 5×10^5 cells/well were plated onto a 6-well plate in a medium containing 5% FBS, incubated for 24 h,infected with KOX or KOX/PEG*b*PHF at 10 (U87) or 2 (U343 and A549) MOI, or mock-infected with PBS as a control, all at pH 7.4 or 6.4. VEGF-containing media were harvested at 48 h after infection, and the secreted VEGF was measured with the abovementioned ELISA kit.

2.7. Cancer cell migration assay

Cancer cell migration was assessed using BD Falcon cell culture inserts containing polyethylene terephthalate membranes (8 μm pore size; BD Biosciences, Bedford, MA). U343 or A549 cells were treated with PBS, KOX, or KOX/PEG*b*PHF (2 MOI) for 24 h, at pH 7.4 or 6.4. Infected cells were placed in the upper chamber of the transwell apparatus and incubated at 37 °C for 4 h.The cells remaining on the upper part of the filter were removed, the filters were stained with eosin, and the migrated cells were counted from eight randomly selected fields.

2.8. Ex vivo assay of aortic ring sprouting

Aortas were obtained from Sprague–Dawley rats (6-weeks-old; Orientbio, Kyunggido, Korea), the surrounding fibroadipose tissues were removed, and the aortas were cut into 1-mm ring segments. The aortic rings were placed on growth-factor-reduced Matrigel (BD Biosciences)-coated plates (48-well), and then overlaid with 50 μL of Matrigel and conditioned media (250 μL) from U343 cells treated with PBS, KOX, or KOX/PEG*b*PHF at

pH 7.4 or 6.4. On day 7,each ring was photographed (×50) and scores from 0 (least positive) to 5 (most positive) were assigned in a double-blinded manner.

2.9. The proton sponge effect of the Ad/PEG*b*PHF complexes

A549 cells were pre-treated with chloroquine (endosome disrupter) at 5 and 20 μM for 30 min. Naked dE1/GFP or dE1/GFP/PEG*b*PHF complexes were then added in the presence or absence of chloroquine for an additional 2 h. Cells were washed with PBS and incubated for 48 h in DMEM/5% FBS. Cells were then visualized by fluorescence microscopy, and GFP expression was quantified by FACS analysis.

2.10. MTT assay

To evaluate the cancer cell killing effects of KOX or KOX/PEG*b*PHF at pH 7.4 or 6.4, U87, U343 and MCF7 cells were grown to 50% confluence in 24-well plates, infected with PBS (control), naked KOX or KOX/PEG*b*PHF (50 MOI for U87 cells, 10 MOI for U343 cells, and 200 MOI for MCF7 cells), and incubated at 37 °C. Two days post-infection, 200 μL of 3-(4,5-dimethylthiazol-2-yl)-2,5-diphenyl-tetrazolium bromide (MTT, 2 mg/mL in PBS; Sigma) was added to each well. The samples were incubated at 37 °C for 4 h, the supernatants were discarded, and the precipitates were dissolved in 1.0 mL dimethylsulfoxide. The plates were read on a microplate reader at 540 nm. The number of living cells in a PBS-treated cell group was analyzed similarly as a negative control.

2.11. Serum stability of KOX complexed with PEG*b*PHF

To evaluate the serum stability, naked KOX or KOX/PEG*b*PHF was mixed with 30% FBS and incubated for 2 or 8 h at 37 °C. U343 or A549 cells were treated with 30% FBS-mixed KOX or KOX/PEG*b*PHF (pH 7.4 and pH 6.4) at an MOI of 10 for 45 min, then media was changed with 5% FBS-contained fresh media. After 48 h of incubation, cell viability was measured by an MTT assay.

2.12. Assessment of antitumor efficacy

To assess the antitumor efficacy of KOX/PEG*b*PHF,subcutaneous U87 tumor xenografts were established by injecting 1×10^7 cells into the abdomens of 6- to 8-week-old male athymic nude mice (Orientbio, Kyunggido, Korea). Once the tumors reached 100–120 mm^3 in volume, mice were randomized into three groups [PBS, KOX, and KOX/PEG*b*PHF] (n=6 per each group) and injected intravenously with 200 μL of PBS or 2×10^{10} VP of KOX or KOX/PEG*b*PHF, three times, every other day. The length (L) and width (W) of each tumor were measured every other day with a caliper, and tumor volume was calculated according to the formula: tumor volume = $0.523\ LW^2$.

2.13. Tumor histology and immunohistochemistry

Tumor tissues were collected from mice at 3 days after the final injection, fixed in 4% formalin, and embedded in paraffin for histological and immunohistochemical examinations. Representative sections were stained with hematoxylin and eosin (H&E) and examined by light microscopy. Tumor sections were also stained with anti-mouse proliferating cell nuclear antigen (PCNA; Dako, Glostrup, Denmark) or anti-rabbit E1A (Santa Cruz

Biotechnology, Santa Cruz, CA) to assess cancer cell proliferation and viral replication, respectively. To measure capillary density, tumor tissue sections were stained with anti-rabbit CD31 IgG (Abcam, Cambridge, MA). After overnight incubation with primary antibodies at 4 °C, tumor sections were treated with an ABC-peroxidase kit (ChemMate DAKO Envision Detection kit). Biotinylated secondary IgG (Santa Cruz Biotechnology) was used for the CD31-specific antibody. Blood vessels in tumors were counted as previously described [38]. The most vascular tumor areas were identified on low power (×100), and vessels were counted from high-power fields (×400). The data are presented as means ± SE for three tumors per group (six different digital images per tumor). All slides were counter-stained with Mayer's hematoxylin.

2.14. Assessing tumor and liver tissue distributions by real-time quantitative PCR

Once the U87 tumor volume reached approximately 100–150 mm^3 in size, tumor-bearing mice were injected intravenously with PBS, KOX, or KOX/PEG*b*PHF (2×10^{10} VP) three times every other day. At 24 h after the third injection, tumor and liver tissues were harvested, and DNA was extracted using a QIAamp DNA mini kit (Qiagen, Hilden, Germany). The number of viral genomes in each sample was assessed by real-time quantitative PCR, as previously described [9].

2.15. Measurement of inflammatory cytokines and liver toxicity

The inflammatory immune response and liver toxicity were examined after systemic injection of PBS, KOX (2×10^{10} VP), or KOX/PEG*b*PHF (2×10^{10} VP). At 6 h post-injection, serum samples were harvested by retroorbital bleeding, and serum interleukin 6 (IL-6) levels were quantified using an IL-6 ELISA kit (R&D Systems). To assess liver toxicity, serum samples were collected at 3 days post-injection, and the alanine aminotransferase (ALT) and aspartate aminotransferase (AST) levels were determined (Neodin Corporation, Seoul, Korea). All of the animal experiments were conducted under the institutional guidelines established for the Hanyang University Institutional Animal Care and Use Committee (IACUC).

2.16. Statistical analysis

Data are expressed as the means ± standard deviation (SD). The Mann–Whitney test was used for statistical comparisons (SPSS 18.0 software; SPSS, Chicago, IL). Differences were considered statistically significant at $P < 0.05$.

3. Results and discussion

3.1. Physicochemical properties of Ad/PEG*b*PHF nanocomplexes

Tumor-microenvironment-sensitive nanoparticles have garnered attention in the field of biomedicine for their ability to easily deliver therapeutic cargoes to a tumor site, leading to enhanced therapeutic efficacy. The block copolymer, methoxy poly(ethylene glycol)-*b*-poly(L-histidine)-poly(L-phenylalanine), herein called PEG*b*PHF, is an amphoteric pH-sensitive polymer in which the imidazole ring has a lone electron pair on the unsaturated nitrogen of histidine [39,40]. The chemical structure of PEG*b*PHF used in this study was confirmed by ^{1}H NMR (Supplementary information Fig. S1). Further, the potential

cytotoxicity of PEG*b*PHF polymer was evaluated by MTT assay (Supplementary information Fig. S2). PEG*b*PHF polymer didn't exhibit apparent cytotoxicity up to the concentration of 100 μg/mL, whereas non-biocompatible poly(ethylenimine) (25K PEI) showed strong toxicity, showing 16.4% and 17% of cell viability at 100 μg/mL concentration on U343 and A549 cells, respectively.

PEG*b*PHF is also fusogenic, meaning that it can disrupt the enveloping membrane of acidic subcellular compartments; this allows it to elicit efficient endosomal escape, resulting in high gene transfer efficiency [41]. Thus, PEG*b*PHF-based vectors are thought to have great potential as an acid-triggered, tumor-microenvironment-specific platform. Here, weused PEG*b*PHFto form a pH-sensitive coating onthe surface of Ads, thereby generating tumor-microenvironment-pH-sensitive complex that we then tested in vitro and in vivo.

We first generated GFP-expressing replication-deficient Ad (dE1/GFP) coated with PEG*b*PHF, dE1/GFP/PEG*b*PHF complex, via electrostatic interaction, and used dynamic light scattering and zeta potentials to measure the average sizes and surface charges obtained with increasing molar ratios of PEG*b*PHF (Fig. 1A). The diameter increased from 111.5 ± 2.54 nm for naked Ad to 306.05 ± 22.27 nm following electrostatic interaction with the maximum PEG*b*PHF:dE1/GFP molar ratio of 1×10^6. The surface charge of the complex also increased from −12 mV ± 1.3 mV (for naked Ad) to 4.77 ± 0.58 mV [for Ad/PEG*b*PHF (molar ratio of 1×10^6)]. Our results indicate that the electrostatic interaction of the cationic PEG*b*PHF polymer with viral particles increased the diameter and zeta potential of the dE1/GFP/PEG*b*PHF complexes in a PEG*b*PHF-molar ratio-dependent fashion. Moreover, to examine the effect of pH on dE1/GFP/PEG*b*PHF complex, we measured the pH-dependent particle size distribution and zeta potentials under various pH ranges (7.4–6.4) (Supplementary information Fig. S3). The average sizes of dE1/GFP/PEG*b*PHF complex were increased with the decrease of pH values, showing 306, 312, 350, 414, and 428 nm at pH 7.4, 7.0, 6.8, 6.6, and 6.4, respectively. The zeta potential value of dE1/GFP/PEG*b*PHF complex was also increased with a decrease of pH, showing 4.77, 5.02, 5.61, 8.58 and 11.25 mV at pH 7.4, 7.0, 6.8, 6.6, and 6.4, respectively. These results imply that pH-responsive PEG*b*PHF copolymer transit pH-dependent micelle–demicelle conversion due to the protonation of imidazole group in the histidine residue, thus increasing both the average size and surface charge of dE1/GFP/PEG*b*PHF complex.

The formation of dE1/GFP/PEG*b*PHF complexes through electrostatic interactions between the negatively charged Ad and the positively charged PEG*b*PHF polymer was further confirmed by a gel-retardation assay. The migration of dE1/GFP/PEG*b*PHF in the gel was increasingly retarded with greater amounts of PEG*b*PHF polymer (Fig. 1B), suggesting that PEG*b*PHF physically binds to the Ad surface with high efficiency. The zeta potential showed that the dE1/GFP/PEG*b*PHF complex had a positive charge when the PEG*b*PHF polymer/Ad molar ratio exceeded 5×10^5. Consistent with these results, when the PEG*b*PHF polymer/Ad molar ratio exceeded 5×10^5, migration towards the anode was blocked and the DNA bands disappeared.

Next, transmission electron microscopy (TEM) imaging was performed at a polymer/Ad molar ratio of 1×10^6, and the morphologies of naked Ad and the dE1/GFP/PEG*b*PHF

complex were compared (Fig. 1C). Our TEM imaging studies revealed that naked Ad had a characteristic hexagonal structure and icosahedral shape, and the Ad particles maintained their original shape when complexed with PEG*b*PHF. These data clearly demonstrate that the negatively charged Ad was adequately complexed with the cationic PEG*b*PHF.

Moreover, the potential cytotoxicity of Ad/PEG*b*PHF nanocomplex was assessed by MTT assay. As shown in Supplementary information Fig. S4, no apparent cytotoxicity was observed in the cells treated with Ad/PEG*b*PHF up to the ratio of 1:1 × 10^6 ratio (Ad:polymer). Furthermore, to know the colloidal stability of the Ad/PEG*b*PHF nanocomplex, we measured particle size distribution of Ad/PEG*b*PHF nanocomplex in PBS buffer at room temperature for 72 h. As shown in Fig. S5, the average size of Ad/PEG*b*PHF nanocomplex was not significantly changed over 72 h, implying that PEG*b*PHF-coated Ad shows good stability under physiological condition.

3.2. The transduction efficiency of Ad/PEG*b*PHF is pH-dependent

To test whether the Ad/PEG*b*PHF nanocomplexes exhibited efficient pH-dependent transduction, GFP expression was measured in CAR-positive and -negative cells. CAR-positive U343 and A549 cells [at a multiplicity of infection (MOI) of 10], and CAR-negative MCF7 cells (100 MOI) were transduced with dE1/GFP or dE1/GFP/PEG*b*PHF at pH 7.4 and 6.4, and at polymer/Ad molar ratios ranging from 5 × 10^4 to 1 × 10^6. As shown in Fig. 2, naked dE1/GFP-transduced U343 or A549 cells exhibited low transgene expression at both of the tested pH values, whereas dE1/GFP/displayed higher transgene expression at pH 6.4 compared to pH 7.4. The level of GFP expression was positively correlated with an increasing polymer/Ad ratio at pH 6.4, demonstrating that this pH-dependent transduction was mediated by the complexed PEG*b*PHF. At pH 6.4, dE1/GFP/PEG*b*PHF showed significantly higher GFP expression than naked Ad in both CAR-positive and -negative cells (526-, 1365-, and 8863-fold increases in U343, A549, and MCF-7 cells, respectively; $P < 0.01$ for U343 and A549 cells, and $P < 0.001$ for MCF7 cells). These results suggest that complexation with PEG*b*PHF could potentially overcome the CAR-dependency of Ad-based cancer therapeutics.

To further characterize the effect of dE1/GFP/PEG*b*PHF on transduction as a function of pH, we transduced U343, A549, and MCF7 cancer cells with dE1/GFP or dE1/GFP/PEG*b*PHF at different pH levels ranging from pH 7.4 to 6.4. As shown in Fig. 3, dE1/GFP/PEG*b*PHF elicited pH-dependent gene transfer, with GFP expression progressively increasing as the pH decreased. This suggests that the ionization of the histidine moiety in PEG*b*PHF increases at a lower pH; this generates a higher net positive charge on the polymer surface, resulting in enhanced cellular uptake. Taken together, these results suggest that Ad/PEG*b*PHF can target regions of low pH (∼pH 6.4), which are a hallmark of the hypoxic tumor microenvironment.

3.3. KOX-expressing oncolytic Ad/PEG*b*PHF downregulates angiogenesis in vitro and ex vivo

Malignant tumors are characterized by hypoxic conditions and high metabolic activity, and fuel their aggressive growth by using an autocrine agent (e.g., VEGF) to trigger

angiogenesis. Thus, we next investigated a dual tumor-targeting therapy by coating the surface of an oncolytic Ad expressing VEGF promoter-targeting transcriptional repressor (KOX), which can suppress VEGF expression, with PEG*b*PHF. We hypothesized that the generated KOX/PEG*b*PHF would target both the hypoxic tumor microenvironment and angiogenic tumor tissues.

To investigate whether KOX/PEG*b*PHF could abrogate VEGF expression in a pH-dependent manner, we infected U87 (10 MOI), U343 (2 MOI) and A549 (2 MOI) cells with naked KOX or KOX/PEG*b*PHF at pH 7.4 or 6.4. In our previous study, we have observed that U87, U343, and A549 cells VEGF at high levels [35]. After 48 h, the media were harvested and ELISA was used to examine VEGF expression (Fig. 4A). In all three cancer cell lines, VEGF expression was more significantly reduced in cells infected with KOX/PEG*b*PHF at pH 6.4, versus cells infected with naked KOX at pH 6.4 or KOX/PEG*b*PHF at pH 7.4 ($P < 0.05$). These results demonstrate that KOX complexed with PEG*b*PHF can suppress VEGF expression in a pH-dependent manner. Next, we investigated whether KOX/PEG*b*PHF could inhibit cancer cell migration and vessel sprouting. As shown in Fig. 4B, infection of U343 cells with KOX/PEG*b*PHF at pH 6.4 inhibited migration (90.9%) more effectively than naked KOX at pH 6.4 (60.2%) or KOX/PEG*b*PHF at pH 7.4 (59.6%) ($P < 0.01$). Similarly, the migration of A549 cells was more significantly inhibited in cells infected with KOX/PEG*b*PHF at pH 6.4 (70.3%) compared to those infected with naked KOX at pH 6.4 (18.4%) or KOX/PEG*b*PHF at pH 7.4 (37.2%) ($P < 0.05$). Microvessel outgrowth was also more significantly attenuated in rat aortic rings treated with conditioned media from U343 cells infected with KOX/PEG*b*PHF at pH 6.4 (no sprout outgrowth; $P < 0.05$) than in those treated with naked KOX at pH 6.4 or KOX/PEG*b*PHF at pH 7.4 (Fig. 4C). Taken together, these data suggest that the KOX oncolytic Ad is still functionally active after complexation with the PEG*b*PHF polymer. Furthermore, the complex shows a potent and pH-dependent antiangiogenic effect that is dramatically stronger at a pH value that is lower than the physiological normal condition.

3.4. Enhanced cell killing and antitumor efficacies are elicited by oncolytic Ad/PEG*b*PHF nanocomplex

To further test whether KOX/PEG*b*PHF can kill cancer cells in a pH-dependent manner and bypass the CAR-dependency of Ad cell entry, we performed MTT assays on CAR-positive (U87 and U343) and CAR-negative (MCF7) cells infected with naked KOX or KOX/PEG*b*PHF at pH 7.4 or pH 6.4. As shown in Fig. 5A, naked KOX elicited effective cell killing in CAR-positive U87 and U343 cells but not CAR-negative MCF7 cells, indicating that it is a CAR-expression-dependent oncolytic Ad. In marked contrast, KOX/PEG*b*PHF at pH 6.4 induced significantly higher cancer cell killing in both CAR-positive and CAR-negative cell lines; we observed 65.6% (U87), 67.5% (U343), and 74.7% (MCF7) killing of cells infected with KOX/PEG*b*PHF at pH 6.4, compared with much lower values for naked KOX (U87, 25.9%; U343, 46.4%; and MCF7, 3.8%) and KOX/PEG*b*PHF at pH 7.4 (U87, 45.3%; U343, 58.6%; and MCF7, 13%). These data demonstrate that KOX/PEG*b*PHF can overcome the lack of CARs that is frequently observed in tumor tissues.

Serum proteins can have a substantial impact on the biological activity of Ad because of highly charged serum proteins. Thus, we evaluate the effect of serum on the stability of Ad by incubating KOX or KOX/PEG*b*PHF in the presence and absence of 30% serum at pH 7.4 or 6.4. As shown in Fig. 5B, the cancer cell killing efficacy of naked KOX was significantly decreased by 24% and 30% in U343 and A549 cells, respectively, after incubation for 8 h in the presence of 30% serum ($P < 0.001$). In marked contrast, the serum did not significantly affect the cancer cell killing efficacy of KOX/PEG*b*PHF at both pH 7.4 and 6.4, demonstrating the stability of PEG*b*PHF-complexed Ad in the presence of serum.

We further assessed whether the sponge effect could be achieved by PEG*b*PHF-complexed Ad system. Chloroquine (CQ),a weak base that increases endosomal and lysosomal pH, causes endosome disruption. Thus, we have used CQ to evaluate the influence of endosomal escape on the overall gene delivery with naked Ad or Ad/PEG*b*PHF nanocomplex. As shown in Fig. S6, the transduction efficiency of naked Ad was significantly increased by CQ, showing 49%($P < 0.01$) and 91% ($P < 0.01$) increase at 5 and 20 μM of CQ concentration, respectively. These results are consistent with previous reports, where CQ was observed to increase the transduction efficiency of Ad [42]. In contrast, CQ did not change the transduction efficiency of Ad/PEG*b*PHF nanocomplex, revealing that this Ad/PEG*b*PHF complex may have its own ability for endosomal escape.

To evaluate the therapeutic value of KOX/PEG*b*PHF in vivo, we established U87 xenograft tumors in mice, and treated the animals with intravenous injections of PBS, KOX, or KOX/PEG*b*PHF. As shown in Fig. 5C, KOX/PEG*b*PHF elicited a significantly greater antitumor activity compared with PBS or KOX. At 22 days post-injection, the volume of the U87 tumor xenografts in mice treated with KOX/PEG*b*PHF was 520 ± 64 mm^3; this was significantly smaller than the corresponding values in the PBS- or KOX-treated control groups (1742 ± 84 mm^3 and 1535 ± 385 mm^3, respectively; $P < 0.05$). These results suggest that the in vivo antitumor activity of KOX was significantly enhanced via systemic administration of KOX/PEG*b*PHF versus naked KOX oncolytic Ad. Together, our findings indicate that KOX/PEG*b*PHF provides a tumor-microenvironment-targeting vector system that can be delivered systematically and may be useful against both primary and metastatic lesions. The increased antitumor effect of KOX/PEG*b*PHF may reflect increased retention in blood circulation, since PEG can decrease non-specific liver uptake and avoid the reticuloenditherial system. Furthermore, the protonation of the imidazole ring in PEG*b*PHF in the low pH tumor microenvironment is likely to facilitate the preferential accumulation and rapid uptake of KOX/PEG*b*PHF into tumor cells.

Ad E1A is a viral replication marker for immunohistochemistry, which detects Ad particles in tumor tissue. The Ad E1A immunohistochemistry results revealed that viral particles were more abundant in tumor tissues from mice treated with Ad/PEG*b*PHF compared to the KOX-treated group, providing additional evidence that KOX/PEG*b*PHF had a better tumor microenvironment-targeting ability than naked KOX (Fig. 5D). Moreover, tumors from KOX/PEG*b*PHF-treated mice displayed larger necrotic areas and fewer viable tumor cells (as revealed by H&E staining) than the tumorsof PBS- or KOX-treated mice. In parallel with these histological results, PCNA antibody staining revealed a dramatic decrease in tumor cell proliferation in tumors of KOX/PEG*b*PHF-treated mice compared with PBS- or KOX-

treated mice. Furthermore, we evaluated anti-angiogenic activity using CD31 staining in tumor tissue. The angiogenic activity was reduced noticeably, with 78.4% and 73.7% lower microvessel densities observed in the tumors of KOX/PEG*b*PHF-treated mice compared to those of PBS- and KOX-treated mice, respectively ($P < 0.01$) (Fig. 5E). These results suggest that systemically delivered KOX/PEG*b*PHF suppresses the expression of VEGF, which is an important component of angiogenesis, thereby triggering potent antiangiogenesis.

To evaluate the liver and tumor tissue distribution profiles of KOX/PEG*b*PHF, mice bearing subcutaneous U87 tumors were treated intravenously three times every other day with KOX or KOX/PEG*b*PHF (2×10^{10} viral particle (VP)). At 24 h after the final injection, tumor and liver tissues were harvested and the DNA levels of the Ad genome were determined by real-time quantitative PCR (Fig. 6). Our results revealed that the liver uptake of KOX/PEG*b*PHF was significantly lower than that of naked KOX, as mice treated with the former showed 668.5-fold lower accumulation in the liver. In contrast, KOX/PEG*b*PHF accumulated at a 189.4-fold higher level in tumor tissues, compared to those of mice treated with naked KOX, resulting in a liver-to-tumor ratio that was 1.3×10^6 higher in mice treated with KOX/PEG*b*PHF versus those treated with naked KOX. As this ratio is an important indicator of the safety and therapeutic value of an agent, these results suggest that KOX/PEG*b*PHF may overcome the limitations of conventional Ad vectors with respect to hepatotoxicity and immunogenicity. Furthermore, the complexes are amenable to intravenous administration, which can be used to treat both primary and disseminated meta-static tumors.

3.5. In vivo safety profile of systemically injected Ad/PEG*b*PHF

Interleukin-6 (IL-6) is often used as a marker for the induction of the innate immune response against Ad. Here, we injected immune-competent Balb/C mice with KOX or KOX/PEG*b*PHF and determined the levels of secreted IL-6 (Fig. 7A). The serum levels of IL-6 in KOX-injected mice were 5.2-fold higher than those of PBS-injected mice, confirming that systemic injection of the naked Ad evoked a strong innate immune response. In contrast, no significant induction of IL-6 was observed among mice injected with either PEG*b*PHF alone or KOX/PEG*b*PHF. This suggests that coating the surface of the KOX oncolytic Ad with PEG*b*PHF can significantly prevent the innate immune response, possibly by masking the hexon and fiber proteins of the Ad.

To investigate the potential hepatotoxicity induced by systemic injection of KOX/PEG*b*PHF, serum alanine aminotransferase (ALT) and aspartate aminotransferase (AST) levels were measured (Fig. 7B). Higher levels of both ALT and AST were detected in KOX-treated mice compared to PBS-treated mice ($P < 0.05$), whereas no elevation of ALT or AST was observed in mice treated with KOX/PEG*b*PHF. This indicates that the complexation of the oncolytic Ad with PEG*b*PHF significantly attenuated the risk of hepatotoxicity. This is in good agreement with our biodistribution study, which showed decreased liver uptake of KOX/PEG*b*PHF compared to naked KOX.

Taken together, our results demonstrate that systemic administration of KOX/PEG*b*PHF elicits enhanced antitumor effects and shows a better safety profile compared to naked KOX. This reflects the preferential tumor accumulation of KOX/PEG*b*PHF, which arises

through its ability to target specific tumor microenvironments, the tendency of cancer cells to support active viral replication, the potent antiangiogenic effects of the loaded agent, the reduced liver uptake of KOX/PEG*b*PHF, and its ability to avoid triggering an immune response. We believe that stimulus-responsive polymers, such as PEG*b*PHF, will support the further development of target-specific platforms for tumor-selective oncolytic therapies.

4. Conclusion

Hypoxic tumor microenvironment-targeting hybrid nanoparticle delivery systems have shown potential as a novel therapeutic strategy, but had not previously been investigated in detail. Here, we generated KOX/PEG*b*PHF, an oncolytic Ad coated with the pH-responsive polymer, PEG*b*PHF. This hybrid vector was designed to treat both primary and metastatic tumors via the ability of the polymer to target the acidic tumor microenvironment, followed by the rapid tumor cellular uptake, active viral replication, and potent antiangiogenic effects of oncolytic Ad. The KOX/PEG*b*PHF complex exhibited better cellular uptake, cancer cell killing effect, and antiangiogenic effects at pH 6.4 compared to normal physiological condition (pH 7.4). Systemic administration of oncolytic Ad/PEG*b*PHF markedly suppressed tumor growth and tumor-specific viral replication in a mouse xenograft model. Additionally, the surface-masked PEG*b*PHF allowed Ad to avoid host immune responses and liver accumulation. The tumor-to-liver ratio (a therapeutic index) of Ad/PEG*b*PHF was significantly increased by 1.3×10^6-fold compared to that of naked Ad in our model. Collectively, these results demonstrate for the first time that Ad/PEG*b*PHF is pH-responsive and targets the hypoxic tumor microenvironment, and could be a safe and effective means for delivering hybrid therapeutic Ad vectors via systemic administration.

Supplementary Material

Refer to Web version on PubMed Central for supplementary material.

Acknowledgments

This work was supported by grants from the National Research Foundation of Korea (2010-0029220, 2013M3A9D3045879, 2013K1A1A2A02050188, Dr. C-O. Yun), the Korea Food and Drug Administration (13172KFDA306, Dr. C-O. Yun), the Basic Research Programs by National Research Foundation of Korea (2013R1A1A2012483, Dr. D. Kasala), and the National Institutes of Health, USA (ROCA177932, Dr. S-W. Kim).

References

1. Post DE, Devi NS, Li Z, Brat DJ, Kaur B, Nicholson A, Olson JJ, Zhang Z, Van Meir EG. Cancer therapy with a replicating oncolytic adenovirus targeting the hypoxic microenvironment of tumors. Clin Cancer Res. 2004; 10:8603–8612. [PubMed: 15623644]
2. Hallden G, Thorne SH, Yang J, Kirn DH. Replication-selective oncolytic adenoviruses. Methods Mol Med. 2004; 90:71–90. [PubMed: 14657560]
3. Heise C, Kirn DH. Replication-selective adenoviruses as oncolytic agents. J Clin Invest. 2000; 105:847–851. [PubMed: 10749561]
4. Kirn D. Replication-selective oncolytic adenoviruses: virotherapy aimed at genetic targets in cancer. Oncogene. 2000; 19:6660–6669. [PubMed: 11426652]
5. Kim J, Kim JH, Choi KJ, Kim PH, Yun CO. E1A- and E1B-Double mutant replicating adenovirus elicits enhanced oncolytic and antitumor effects. Hum Gene Ther. 2007; 18:773–786. [PubMed: 17725410]

6. Ries SJ, Brandts CH, Chung AS, Biederer CH, Hann BC, Lipner EM, McCormick F, Korn WM. Loss of p14ARF in tumor cells facilitates replication of the adenovirus mutant dl1520 (ONYX-015). Nat Med. 2000; 6:1128–1133. [PubMed: 11017144]
7. Green M, Daesch GE. Biochemical studies on adenovirus multiplication. II. Kinetics of nucleic acid and protein synthesis in suspension cultures. Virology. 1961; 13:169–176. [PubMed: 13708189]
8. Kafri T, Morgan D, Krahl T, Sarvetnick N, Sherman L, Verma I. Cellular immune response to adenoviral vector infected cells does not require de novo viral gene expression: implications for gene therapy. Proc Natl Acad Sci U S A. 1998; 95:11377–11382. [PubMed: 9736744]
9. Kim PH, Sohn JH, Choi JW, Jung Y, Kim SW, Haam S, Yun CO. Active targeting and safety profile of PEG-modified adenovirus conjugated with herceptin. Biomaterials. 2011; 32:2314–2326. [PubMed: 21227505]
10. Cunningham CC, Chada S, Merritt JA, Tong A, Senzer N, Zhang Y, Mhashilkar A, Parker K, Vukelja S, Richards D, Hood J, Coffee K, Nemunaitis J. Clinical and local biological effects of an intratumoral injection of mda-7 (IL24; INGN 241) in patients with advanced carcinoma: a phase I study. Mol Ther. 2005; 11:149–159. [PubMed: 15585416]
11. Cichon G, Schmidt HH, Benhidjeb T, Loser P, Ziemer S, Haas R, Grewe N, Schnieders F, Heeren J, Manns MP, Schlag PM, Strauss M. Intravenous administration of recombinant adenoviruses causes thrombocytopenia, anemia and erythroblastosis in rabbits. J Gene Med. 1999; 1:360–371. [PubMed: 10738553]
12. Danielsson A, Elgue G, Nilsson BM, Nilsson B, Lambris JD, Totterman TH, Kochanek S, Kreppel F, Essand M. An ex vivo loop system models the toxicity and efficacy of PEGylated and unmodified adenovirus serotype 5 in whole human blood. Gene Ther. 2010; 17:752–762. [PubMed: 20220781]
13. Alemany R, Suzuki K, Curiel DT. Blood clearance rates of adenovirus type 5 in mice. J Gen Virol. 2000; 81:2605–2609. [PubMed: 11038370]
14. Kasala D, Choi JW, Kim SW, Yun CO. Utilizing adenovirus vectors for gene delivery in cancer. Expert Opin Drug Deliv. 2014; 11:379–392. [PubMed: 24392755]
15. Croyle MA, Chirmule N, Zhang Y, Wilson JM. “Stealth” adenoviruses blunt cell-mediated and humoral immune responses against the virus and allow for significant gene expression upon readministration in the lung. J Virol. 2001; 75:4792–4801. [PubMed: 11312351]
16. Gao JQ, Eto Y, Yoshioka Y, Sekiguchi F, Kurachi S, Morishige T, Yao X, Watanabe H, Asavatanabodee R, Sakurai F, Mizuguchi H, Okada Y, Mukai Y, Tsutsumi Y, Mayumi T, Okada N, Nakagawa S. Effective tumor targeted gene transfer using PEGylated adenovirus vector via systemic administration. J Control Release. 2007; 122:102–110. [PubMed: 17628160]
17. Lee WJ, Kim YO, Choi IK, Rah DK, Yun CO. Adenovirus-relaxin gene therapy for keloids: implication for reversing pathological fibrosis. Br J Dermatol. 2011; 165:673–677. [PubMed: 21623756]
18. Kim PH, Kim TI, Yockman JW, Kim SW, Yun CO. The effect of surface modification of adenovirus with an arginine-grafted bioreducible polymer on transduction efficiency and immunogenicity in cancer gene therapy. Biomaterials. 2010; 31:1865–1874. [PubMed: 19962189]
19. Fisher KD, Seymour LW. HPMA copolymers for masking and retargeting of therapeutic viruses. Adv Drug Deliv Rev. 2010; 62:240–245. [PubMed: 20005911]
20. Kopecek J, Kopeckova P. HPMA copolymers: origins, early developments, present, and future. Adv Drug Deliv Rev. 2010; 62:122–149. [PubMed: 19919846]
21. Eto Y, Gao JQ, Sekiguchi F, Kurachi S, Katayama K, Maeda M, Kawasaki K, Mizuguchi H, Hayakawa T, Tsutsumi Y, Mayumi T, Nakagawa S. PEGylated adenovirus vectors containing RGD peptides on the tip of PEG show high transduction efficiency and antibody evasion ability. J Gene Med. 2005; 7:604–612. [PubMed: 15543536]
22. Maeda M, Kida S, Hojo K, Eto Y, Gaob JQ, Kurachi S, Sekiguchi F, Mizuguchi H, Hayakawa T, Mayumi T, Nakagawa S, Kawasaki K. Design and synthesis of a peptide-PEG transporter tool for carrying adenovirus vector into cells. Bioorg Med Chem Lett. 2005; 15:621–624. [PubMed: 15664825]

23. Lanciotti J, Song A, Doukas J, Sosnowski B, Pierce G, Gregory R, Wadsworth S, O'Riordan C. Targeting adenoviral vectors using heterofunctional polyethylene glycol FGF2 conjugates. Mol Ther. 2003; 8:99–107. [PubMed: 12842433]
24. Green NK, Morrison J, Hale S, Briggs SS, Stevenson M, Subr V, Ulbrich K, Chandler L, Mautner V, Seymour LW, Fisher KD. Retargeting polymer-coated adenovirus to the FGF receptor allows productive infection and mediates efficacy in a peritoneal model of human ovarian cancer. J Gene Med. 2008; 10:280–289. [PubMed: 18214996]
25. Kwon OJ, Kang E, Choi JW, Kim SW, Yun CO. Therapeutic targeting of chitosan-PEG-folate-complexed oncolytic adenovirus for active and systemic cancer gene therapy. J Control Release. 2013; 169:257–265. [PubMed: 23562633]
26. Denison TA, Bae YH. Tumor heterogeneity and its implication for drug delivery. J Control Release. 2012; 164:187–191. [PubMed: 22537887]
27. Baker A, Saltik M, Lehrmann H, Killisch I, Mautner V, Lamm G, Christofori G, Cotten M. Polyethylenimine (PEI) is a simple, inexpensive and effective reagent for condensing and linking plasmid DNA to adenovirus for gene delivery. Gene Ther. 1997; 4:773–782. [PubMed: 9338005]
28. Vetter A, Virdi KS, Espenlaub S, Rodl W, Wagner E, Holm PS, Scheu C, Kreppel F, Spitzweg C, Ogris M. Adenoviral vectors coated with PAMAM dendrimer conjugates allow CAR independent virus uptake and targeting to the EGF receptor. Mol Pharm. 2013; 10:606–618. [PubMed: 23281933]
29. Kawamata Y, Nagayama Y, Nakao K, Mizuguchi H, Hayakawa T, Sato T, Ishii N. Receptor-independent augmentation of adenovirus-mediated gene transfer with chitosan in vitro. Biomaterials. 2002; 23:4573–4579. [PubMed: 12322978]
30. Kim J, Li Y, Kim SW, Lee DS, Yun CO. Therapeutic efficacy of a systemically delivered oncolytic adenovirus — biodegradable polymer complex. Biomaterials. 2013; 34:4622–4631. [PubMed: 23541109]
31. Varkouhi AK, Scholte M, Storm G, Haisma HJ. Endosomal escape pathways for delivery of biologicals. J Control Release. 2011; 151:220–228. [PubMed: 21078351]
32. Verma A, Stellacci F. Effect of surface properties on nanoparticle–cell interactions. Small. 2010; 6:12–21. [PubMed: 19844908]
33. Lee ES, Na K, Bae YH. Polymeric micelle for tumor pH and folate-mediated targeting. J Control Release. 2003; 91:103–113. [PubMed: 12932642]
34. Kim GM, Bae YH, Jo WH. pH-induced micelle formation of poly(histidine-co-phenylalanine)-block-poly(ethylene glycol) in aqueous media. Macromol Biosci. 2005; 5:1118–1124. [PubMed: 16245269]
35. Kang YA, Shin HC, Yoo JY, Kim JH, Kim JS, Yun CO. Novel cancer antiangiotherapy using the VEGF promoter-targeted artificial zinc-finger protein and oncolytic adenovirus. Mol Ther. 2008; 16:1033–1040. [PubMed: 18398429]
36. Lee CH, Kasala D, Na Y, Lee MS, Kim SW, Jeong JH, Yun CO. Enhanced therapeutic efficacy of an adenovirus-PEI-bile-acid complex in tumors with low coxsackie and adenovirus receptor expression. Biomaterials. 2014; 35:5505–5516. [PubMed: 24731708]
37. Mittereder N, March KL, Trapnell BC. Evaluation of the concentration and bioactivity of adenovirus vectors for gene therapy. J Virol. 1996; 70:7498–7509. [PubMed: 8892868]
38. de Jong JS, van Diest PJ, Baak JP. Heterogeneity and reproducibility of microvessel counts in breast cancer. Lab Invest. 1995; 73:922–926. [PubMed: 8558855]
39. Lee ES, Shin HJ, Na K, Bae YH. Poly(l-histidine)-PEG block copolymer micelles and pH-induced destabilization. J Control Release. 2003; 90:363–374. [PubMed: 12880703]
40. Taluja A, Bae YH. Role of a novel excipient poly(ethylene glycol)-b-poly(l-histidine) in retention of physical stability of insulin in aqueous solutions. Pharm Res. 2007; 24:1517–1526. [PubMed: 17385016]
41. Chang KL, Higuchi Y, Kawakami S, Yamashita F, Hashida M. Efficient gene transfection by histidine-modified chitosan through enhancement of endosomal escape. Bioconjug Chem. 2010; 21:1087–1095. [PubMed: 20499901]

42. Hoque AT, Baccaglini L, Baum BJ. Hydroxychloroquine enhances the endocrine secretion of adenovirus-directed growth hormone from rat submandibular glands in vivo. Hum Gene Ther. 2001; 12:1333–1341. [PubMed: 11440626]

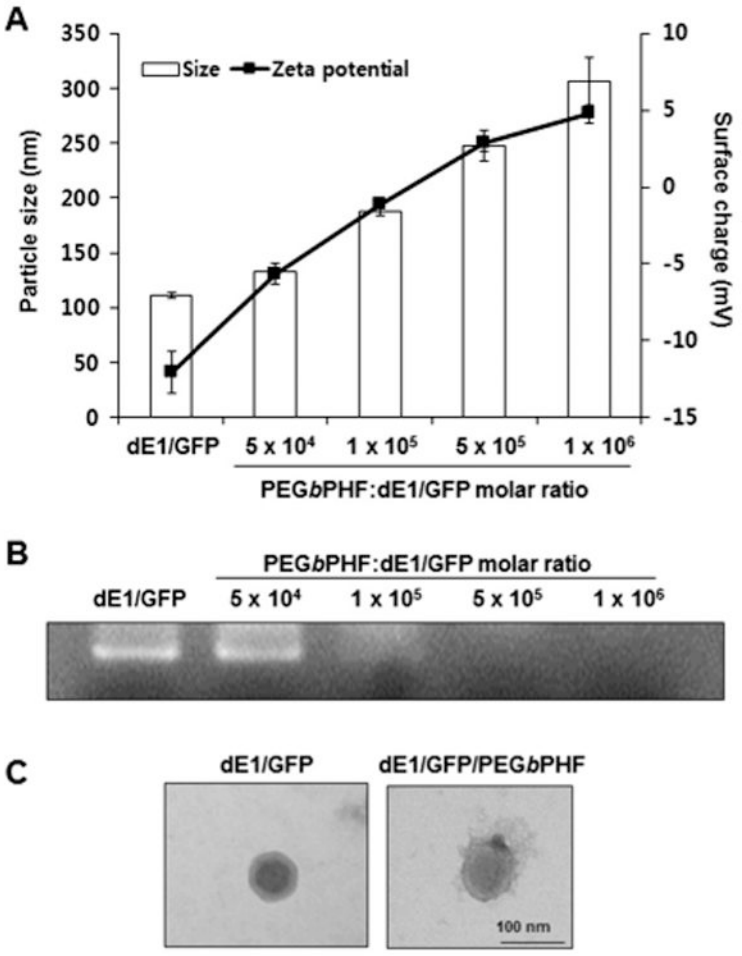

Fig. 1.

Physicochemical properties of dE1/GFP/PEG*b*PHF nanocomplexes. (A) The average size (nm) and zeta-potential value (mV) of PEG*b*PHF-coated dE1/GFP (1×10^{10} VP) were measured at various molar ratios of PEG*b*PHF polymer/Ad (pH 7.4). The data represent the means ± SD for three replicates. (B) Gel-retardation assay of dE1/GFP/PEG*b*PHF complexes containing various molar ratios of PEG*b*PHF polymer/Ad (pH 7.4). (C) TEM images of naked dE1/GFP and dE1/GFP/PEG*b*PHF complexes at 1×10^6 PEG*b*PHF/Ad particle in PBS buffer (pH 7.4).

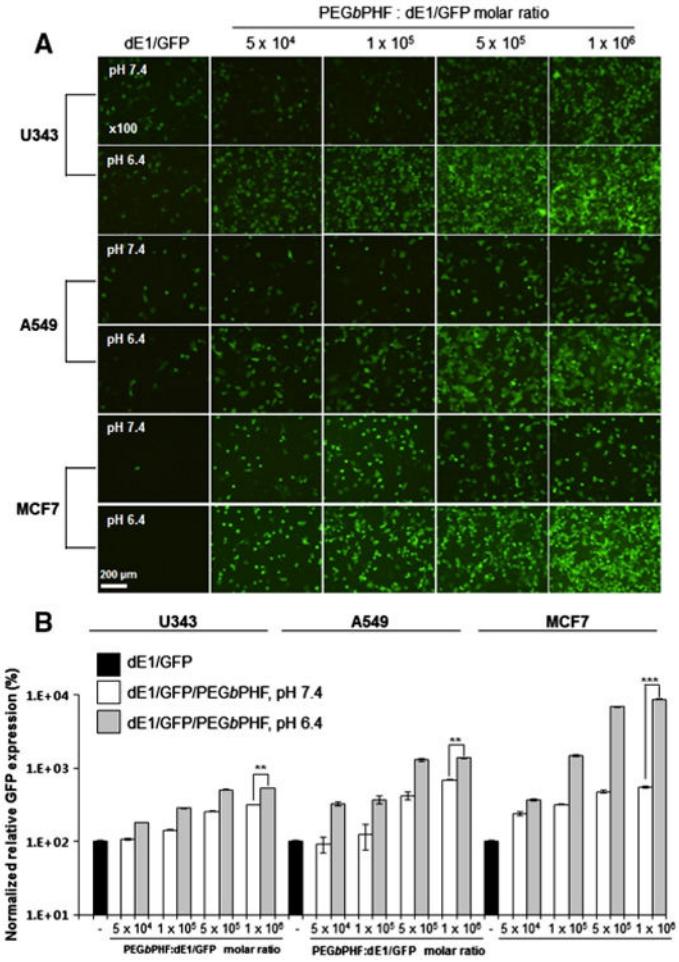

Fig. 2.

The transduction efficiency of dE1/GFP/PEG*b*PHF depends on the PEG*b*PHF/Ad molar ratio at pH 7.4 and 6.4. (A) Fluorescence images of dE1/GFP or dE1/GFP/PEG*b*PHF complexes. Ad particles (1×10^{10} VP) were complexed with various molar ratios of PEG*b*PHF (5×10^4, 1×10^5, 5×10^5, or 1×10^6). U343, A549 or MCF7 cells were transduced for 30 min with naked dE1/GFP or dE1/GFP/PEG*b*PHF at pH 7.4 or 6.4. At 48 h after transduction, GFP images were observed under a fluorescence microscope. Original magnification: × 100. (B) Quantitative FACS analysis of GFP expression. The normalized transduction efficiency of dE1/GFP/PEG*b*PHF complexes relative to dE1/GFP was expressed as the fold increase relative to naked dE1/GFP. The data are presented as the means ± SD of triplicate experiments. Symbols: $^{**}P < 0.01$, $^{***}P < 0.001$ versus dE1/GFP/PEG*b*PHF at pH 7.4.

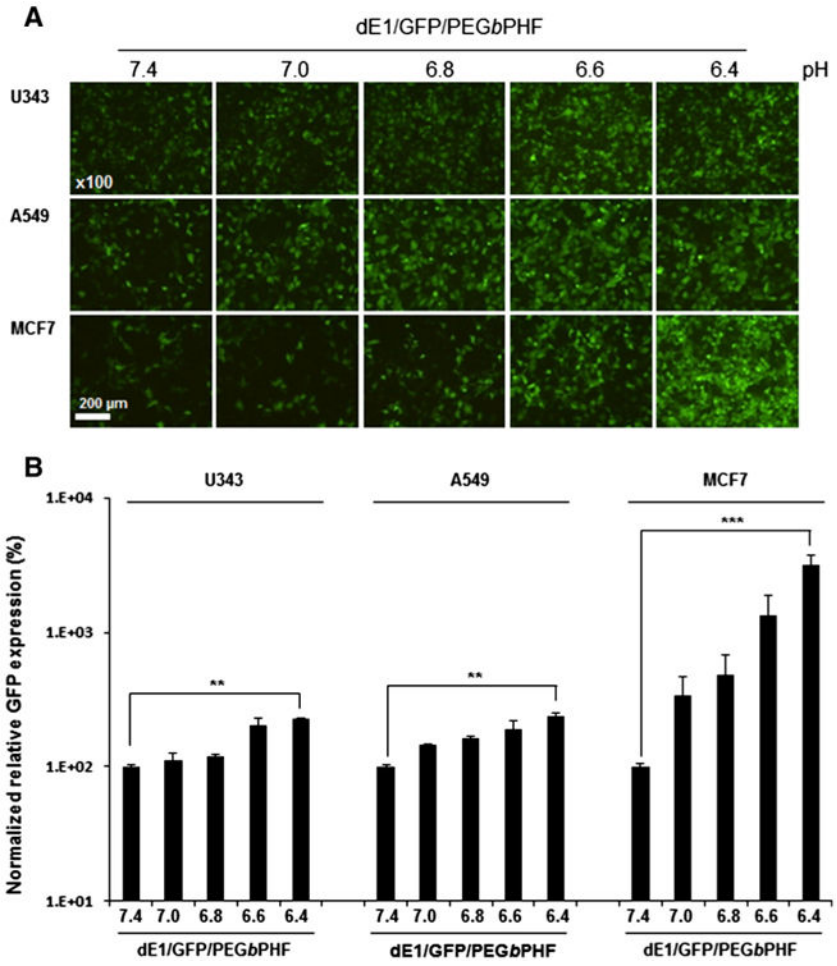

Fig. 3.

The transduction efficiency of dE1/GFP/PEG*b*PHF is pH-dependent. (A) Fluorescence images of dE1/GFP/PEG*b*PHF complexes (1×10^6/Ad molar ratio). U343, A549 or MCF7 cells were transduced with naked dE1/GFP or dE1/GFP/PEG*b*PHF complexes at various pH levels (7.4, 7.0, 6.8, 6.6, and 6.4) for 30 min. At 48 h after transduction, GFP images were observed under a fluorescence microscope. Original magnification: × 100. (B) Quantitative FACS analysis of GFP expression. The normalized transduction efficiency of dE1/GFP/PEG*b*PHF complexes relative to dE1/GFP was expressed as the fold increase versus naked dE1/GFP. The data represent the means ± SD of triplicate experiments. Symbols: $^{**}P < 0.01$, $^{***}P < 0.001$ versus dE1/GFP/PEG*b*PHF at pH 7.4.

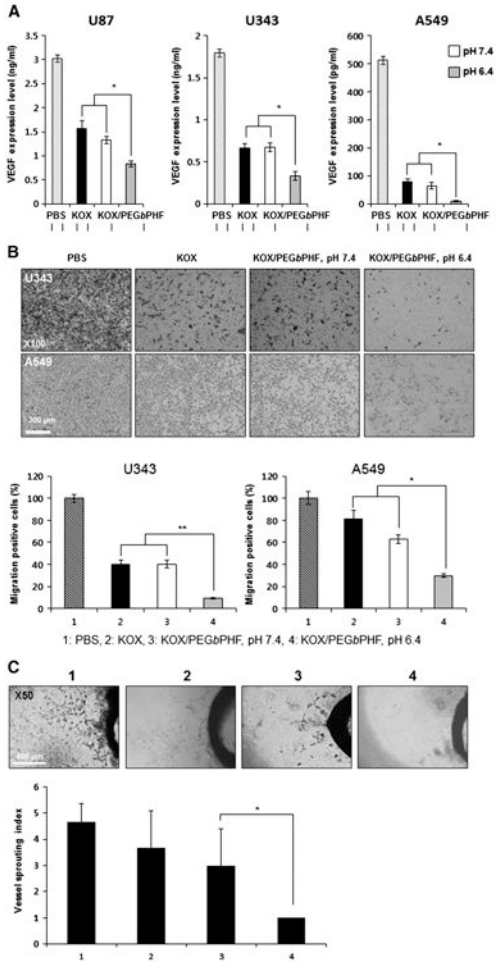

Fig. 4.

Potent antiangiogenic effects of KOX/PEG*b*PHF. (A) U87, U343 and A549 cells were infected with PBS, KOX or KOX/PEG*b*PHF at pH 7.4 or 6.4. At 48 h after infection, the VEGF concentration in each culture supernatant was measured by ELISA. The data are presented as means± SD (n = 3);**P*< 0.05 versus KOX and KOX/PEG*b*PHF at pH 7.4. (B) U343 and A549 cells were infected with PBS, KOX or KOX/PEG*b*PHF at pH 7.4 or 6.4. At 24 h after infection, cells were detached and placed in the upper chamber of the transwell apparatus. Following 4 h of incubation, migrated cells (those found on the lower filter surface) were stained with eosin and counted (×100) from eight randomly selected fields. The results obtained with PBS-treated cells were set to 100%. The results are given as the means ± SD of eight independent fields. Symbols: **P* < 0.05, ***P* < 0.01 versus KOX at KOX/PEG*b*PHF at pH 7.4. (C) Aortic rings were cultured in Matrigel with conditioned medium from cancer cells infected with PBS, KOX, or KOX/PEG*b*PHF at pH 7.4 or 6.4 for 7 days, and photographed (×50). The vessel-sprouting index was graded from 0 (least positive) to 5 (most positive), and the data are indicated as means ± SD (n = 3). Symbol: **P* < 0.05 versus KOX/PEG*b*PHF at pH 7.4.

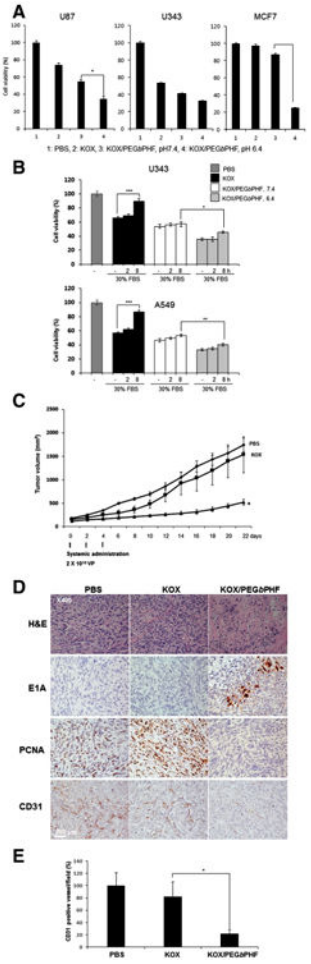

Fig. 5.

Enhanced cancer cell killing and antitumor effects of KOX/PEG*b*PHF. (A) U87, U343 and MCF7 cells were infected with KOX or KOX/PEG*b*PHF at pH 7.4 or 6.4. Cell viability was assessed by MTT assay. The PBS-treated group (control) was set at 100%. The data are presented as the means ± SD of triplicate experiments. Symbol: ***$P < 0.001$ versus KOX/PEG*b*PHF at pH7.4. (B) Cancer cell killing effect of KOX or KOX/PEG*b*PHF complex in the presence and absence of 30% FBS. Cell viability was assessed by an MTT assay. The PBS-treated control group was set at 100%. Data represent the means and standard deviations of triplicate experiments. ***$P < 0.001$ versus the absence of 30% FBS, pH 7.4. (C) Subcutaneous tumors derived from implanted U87 cells were treated with PBS, KOX (2×10^{10} VP) or KOX/PEG*b*PHF (2×10^{10} VP) three times every other day. Tumor volume was measured every two days following treatment. The arrows indicate the points of treatment. The results are expressed as means ± SD (n = 6 per group). Symbol: *$P < 0.05$ versus KOX. (D) Representative tumor tissues were stained with H&E, E1A, PCNA, or CD31 to detect necrosis, viral replication, tumor cell proliferation, and blood vessels, respectively. (E) Vessels were counted in tumor tissues for each treatment group. Six images were analyzed per group, and all data are shown as means ± SD. Symbol:*$P < 0.05$ versus KOX.

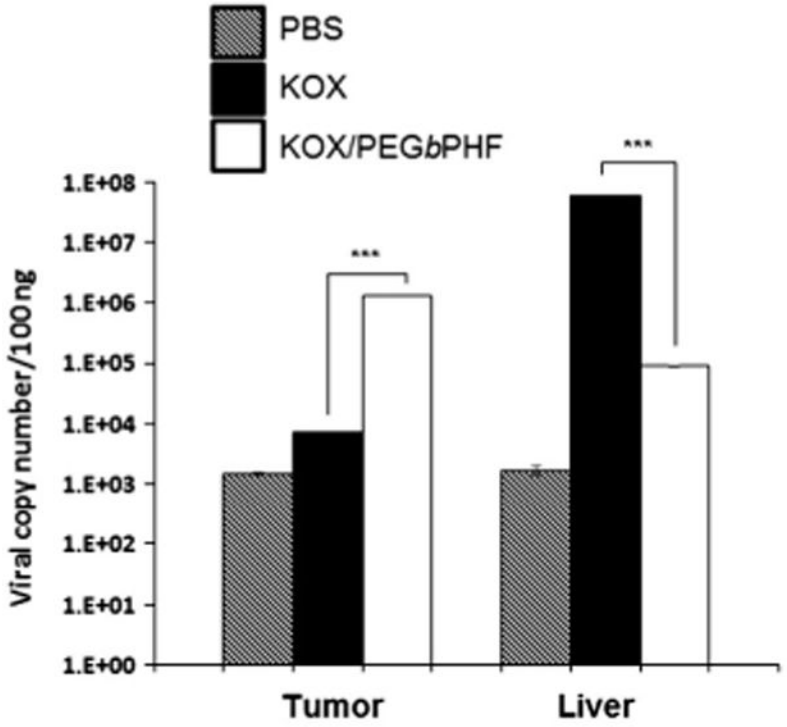

Normalized tumor to liver ratio	
KOX	1
KOX/PEG*b*PHF	1.3 x 10^6

Fig. 6.

Distribution profiles of naked KOX and KOX/PEG*b*PHF in tumor and liver tissues. Once the U87 tumor volume reached approximately 100–150 mm^3, PBS, KOX or KOX/PEG*b*PHF (2×10^{10} VP) was systemically injected three times every other day. Tumor and liver tissues were harvested at 24 h post-injection, and real-time quantitative PCR was performed to detect Ad genomic DNA. The data are expressed as the copy number of the Ad E1A gene. Data represent means ± SD; n = 3 for each experimental condition. Symbol: ***$P < 0.001$ versus KOX.

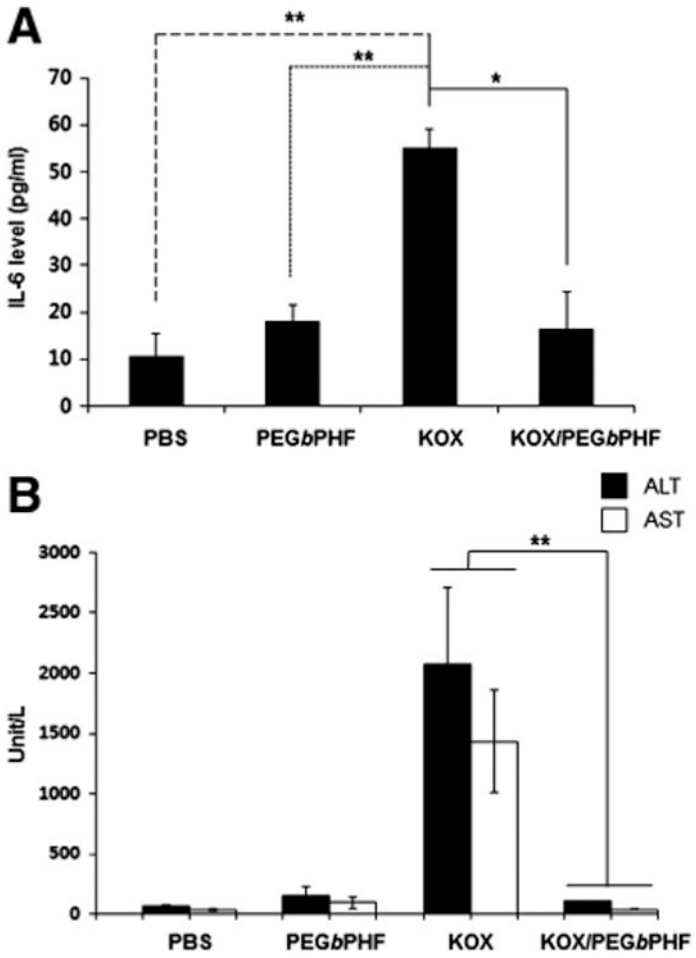

Fig. 7.

Assessment of the immune responsiveness and hepatotoxicity of KOX/PEG*b*PHF. (A) Induction of the inflammatory cytokine, IL-6. At 6 h after intravenous injection of PBS, PEG*b*PHF, KOX(2×10^{10} VP) or KOX/PEG*b*PHF (2×10^{10} VP), serum samples was collected and IL-6 levels were measured by ELISA. Data represent means ± SD; n = 3 for each experimental condition. Symbols: $^{**}P < 0.01$ and $^{*}P < 0.05$ versus KOX. (B) Serum ALT and AST were measured at 72 h after intravenous administration of PBS, PEG*b*PHF, naked KOX (2×10^{10} VP),orKOX/PEG*b*PHF (2×10^{10} VP). Data represent means ± SD; n = 3 for each experimental condition. Symbol: $^{**}P<0.01$ versus KOX.